Neuroscience 310 (2015) 198–205

CONTRAST ADAPTATION IS SPATIAL FREQUENCY SPECIFIC IN MOUSE PRIMARY VISUAL CORTEX

J. L. KING, M. P. LOWE AND N. A. CROWDER*

Department of Psychology and Neuroscience, Dalhousie University, Halifax, NS, Canada

Abstract—Contrast adaptation, generated by prolonged viewing of a high contrast spatial pattern, is known to reduce perceptual sensitivity to subsequently presented stimuli of similar spatial frequency (SF). Neural correlates of this pattern-specific contrast adaptation have been described in several classic studies in cat primary visual cortex (V1). These results have also recently been extended to mice, which is a genetically manipulable animal model. Here we attempt to parse the potential mechanisms contributing to this phenomenon by determining whether the SF specificity of contrast adaptation observed in mouse V1 neurons depends on the spike rate elicited by the adapting gratings. We found that adapting stimuli that drove a neuron more strongly generally produced more adaptation, implicating an intrinsic or fatigue-like process. Importantly, we also observed that slightly stronger contrast adaptation was produced when the adapting SF matched the test SF even when matched and nonmatched adapting gratings elicited similar spike rates indicating extrinsic or network processes contribute as well.

Key words: vision, sinusoidal gratings, spatial frequency, contrast adaptation, animal model, electrophysiology.

INTRODUCTION

In vision research, spatial contrast is defined as relative luminance across space. This stimulus attribute, henceforth referred to simply as contrast, is processed in the visual system as early as center-surround antagonism in the retina (Kaplan and Shapley, 1986). Contrast is critical for the detection of edges that can define object borders, textures, lighting conditions and shadows. There is perceptual and physiological evidence that the visual system possesses several self-calibration mechanisms to quickly adjust its sensitivity to contrast according to the recent stimulus history, and this is called contrast adaptation (see Kohn, 2007 for a recent review).

Perceptual studies of contrast adaptation show that prolonged viewing of a high-contrast adapting pattern can produce a perceived fading of the adapting stimulus and reduce sensitivity to subsequently presented low contrast test stimuli, but it can also improve discrimination around the adapting contrast (Blakemore and Campbell, 1969b; Greenlee and Heitger, 1988; Foley and Chen, 1997; Abbonizio et al., 2002). Of particular interest is the finding that contrast adaptation is strongest when the spatial frequency (SF) of the test stimulus matches that of the adapting stimulus (Blakemore and Campbell, 1969a,b; Blakemore and Nachmias, 1971; Blakemore et al., 1973; Snowden and Hammett, 1996). This pattern-specificity may provide clues about the possible mechanisms underlying contrast adaptation.

The neurophysiological correlates of perceptual adaptation have most frequently been studied in the primary visual cortex (V1) of cats and primates. V1 neurons have sigmoidal contrast response functions when the spike rate is plotted against stimulus contrast, and adaptation to a high contrast pattern causes this function to shift rightward and center the steepest part of the curve near the adapting contrast (Movshon and Lennie, 1979; Ohzawa et al., 1982, 1985; Sclar et al., 1989; Bonds, 1991; Ibbotson, 2005). As with psychophysical studies, the magnitude of adaptation shown by V1 neurons depends on the SF of the adapting and test stimuli (Movshon and Lennie, 1979; Ohzawa et al., 1985; Saul and Cynader, 1989), although this may not be the case for antecedent areas such as the dorsal lateral geniculate nucleus (dLGN; Duong and Freeman, 2007).

We recently explored pattern selectivity of contrast adaptation in mouse V1 with the aim of establishing similarities between a genetically tractable species and more traditional animal models of vision (LeDue et al., 2013). Neurons in mouse V1 share several properties with those described in cats and primates including retinotopic organization, orientation selectivity, and most important for this work, SF tuning and contrast adaptation (Kalatsky and Stryker, 2003; Niell and Stryker, 2008; Stroud et al., 2012). When mouse V1 neurons were tested at their preferred SF they adapted more when the adapting grating matched the test grating, which provides evidence of SF-specificity of contrast adaptation similar to what occurs in other species. Several explana-

*Corresponding author. Address: Dalhousie University, Department of Psychology and Neuroscience, 1355 Oxford Street, PO Box 15000, Halifax, NS B3H 4R2, Canada. Tel: +1-902-494-6025; fax: +1-902-494-6585.
E-mail address: nathan.crowder@dal.ca (N. A. Crowder).

Abbreviations: AUC, area under the curve; cpd, cycles per degree; dLGN, dorsal lateral geniculate nucleus; F_0, mean time-averaged response; F_1, first Fourier coefficient of the response; M, matched adaptation; N.M., nonmatched adaptation; SDFs, spike density functions; SF, spatial frequency; TF, temporal frequency; V1, primary visual cortex.

http://dx.doi.org/10.1016/j.neuroscience.2015.09.037
0306-4522/

tions of how this specificity might occur have been raised in previous work in cats. The test stimuli of LeDue et al. (2013) were always presented at each neuron's peak SF, and matched adaptation (adapting SF = test SF) elicited higher spike rates than nonmatched adaptation (adapting SF ≠ test SF), so this specificity might reflect an intrinsic or fatigue-like process where higher firing rates elicited by preferred stimuli produce more adaptation (as proposed by Vautin and Berkley, 1977). Conversely, several examples of robust adaptation arising from stimuli that do not evoke strong responses indicate specificity need not be rooted in fatigue (e.g. Ohzawa et al., 1985; Crowder et al., 2006; Dhruv et al., 2011). In these cases adaptation is proposed to come from sources extrinsic to the recorded neuron, such as being inherited from broadly tuned afferents or implemented through local cortical networks.

In the present study we attempted to disambiguate possible mechanisms underlying contrast adaptation by examining SF-specificity of adaptation using adapting gratings that elicited approximately equal firing rates. For each mouse V1 neuron, two adapting SFs were selected that straddled the neuron's peak SF, and the test grating SF was matched to one of these stimuli. We found that when spike rates were equated between matched and nonmatched adaptation, thereby equalizing any potential intrinsic or fatigue-like processes, SF-specificity of contrast adaptation was still present but substantially weaker than previously reported.

EXPERIMENTAL PROCEDURES

Animals

Experiments were performed on male C57BL/6J mice, aged 2–7 months, weighing between 22 and 33 g (n = 14). All experimental procedures were conducted in accordance with the guidelines of the Canadian Council on Animal Care and were approved by the Dalhousie University Committee on Laboratory Animals.

Physiological preparation

Animals were pre-medicated with an injection of chlorprothixene (Sigma Aldrich, 5 mg/kg, i.p.), then placed in a custom face-mask and anesthetized with isoflurane in oxygen for the remainder of the experiment (2.5% isoflurane during induction, 1.5% during surgery and 0.5% during recording; Pharmaceutical Partners of Canada). Additional doses of chlorprothixene were given every four hours. Once anesthetized, mice were maintained at a body temperature of 37.5 °C using a heating pad, and their corneas were protected by frequent application of optically neutral silicone oil (30,000 cSt, Sigma Aldrich). Pupils were not dilated so there was presumably a large depth of focus, and paralysis was not induced because previous electrophysiological studies of mouse V1 have found eye movements under anesthesia are negligible (Wang and Burkhalter, 2007; Niell and Stryker, 2008; Gao et al., 2010).

To expose V1, the scalp was removed, a head post was secured using dental epoxy, then a craniotomy (~1 mm^2) was made 0.8 mm anterior and 2.3 mm lateral to lambda (Paxinos and Franklin, 2001). The craniotomy was filled with warm saline to prevent dehydration of the cortical surface. Extracellular recordings were made with glass micropipettes that were filled with 2 M NaCl and had a tip diameter of 2–3 μm. Signals from individual cells were isolated, amplified, filtered, and acquired with a CED 1401 interface and Spike2 software (Cambridge Electronic Designs, Cambridge, UK) sampled at 25 kHz. Online analyses were performed on the transistor–transistor logic (TTL) output from a window discriminator (Dagan, Minneapolis, MN, USA), but spike sorting and all subsequent analyses were performed offline.

Visual stimuli

Once a visually responsive neuron was isolated, the receptive field was mapped manually with bars and spots produced with an ophthalmoscope. Computer generated visual stimuli were programed in MATLAB (Math Works, Natick, MA, USA) using the Psychophysics Toolbox extension (Brainard, 1997; Pelli, 1997), and were presented on a calibrated CRT monitor (LG Flatron 915FT Plus 19 inch display, 100 Hz refresh, 1024 × 768 pixels, mean luminance = 30 cd/m^2) at a viewing distance of 15–30 cm. All stimuli were presented for 8–12 repetitions.

On-line tuning functions for orientation preference, receptive field size, and spatio-temporal tuning were calculated to select appropriate stimulus parameters for the adaptation protocol. Orientation selectivity was tested with square-wave gratings of 8 orientations presented in random order (22.5° spacing). For each orientation, the grating first appeared and remained stationary for 0.5 s, then drifted in one direction for 2 s, then paused for 0.5 s, then drifted in the opposite direction for 2 s, then paused for a final 0.5 s. Preferred stimulus size was tested in two ways: (1) with a circular aperture containing a sine-wave grating; and (2) with a full field grating with a circular aperture of gray in the center. Six different stimulus diameters were presented for 2 s each in random order (8°, 12°, 24°, 32°, 48°, 64°). In addition to testing size tuning, these stimuli served as a confirmation that the monitor was centered on the neuron's receptive field. The stimulus size used for subsequent tests was chosen as either the diameter where the size tuning function began to asymptote in neurons lacking surround suppression, or the peak of the function for neurons that showed surround suppression. Preferred spatial and temporal frequencies (TF) for each neuron were determined with sine-wave gratings of the preferred orientation and drift direction presented in an aperture of the preferred size. Thirty-six combinations of SFs (0.01, 0.02, 0.04, 0.08, 0.16, 0.32 cycles per degree (cpd)) and TFs (0.25, 0.50, 1, 2, 4, 8 Hz) were presented for 2 s each in random order. A gray of mean luminance was presented for 0.5 s between all grating stimuli used to generate on-line tuning functions.

A top-up contrast adaptation protocol was used to facilitate comparisons with previous mouse experiments, as well as original experiments performed in cats and primates (Movshon and Lennie, 1979; Duong and

Freeman, 2007; Dhruv et al., 2011; Stroud et al., 2012; LeDue et al., 2013). Sine-wave contrast is defined as:

$$\text{Michelson contrast} = \frac{\text{Luminance}_{max} - \text{Luminance}_{min}}{\text{Luminance}_{max} + \text{Luminance}_{min}} \quad (1)$$

where Luminance_{max} and Luminance_{min} are the maximum and minimum luminance, respectively. All adaptation stimuli were presented at the neuron's preferred orientation and drift direction, size, and TF. Based on the on-line spatiotemporal tuning function of each neuron, two SFs that straddled the peak SF and elicited approximately equal firing rates were selected for the adapting stimuli. In practice, the selected SFs were always at least one octave apart, and most often differed by 2 octaves. Contrast adaptation was measured in blocks, and the SF of the test gratings (usually the higher of the two SFs) was the same across all blocks. Non-adapted contrast response functions were measured with ten contrasts (0.04, 0.08, 0.12, 0.16, 0.24, 0.32, 0.48, 0.64, 0.82, 1) presented in random order for 0.5 s tests, with 4 s of mean luminance between stimuli (Fig. 1A black lines). Adaptation blocks started with 60 s of the adapting grating at 0.2–0.32 contrast, followed by 0.5 s tests (aforementioned contrasts) interleaved with 4 s top-ups of the adapting grating. Two adapted contrast response functions were collected: (1) in the "matched adaptation" block, the SF of the adapting grating was the same as the SF of the test grating (Fig. 1A red lines); (2) in the "nonmatched adaptation" block, the SF of the adapting grating differed from the SF of the test grating (although they elicited similar spike rates; Fig. 1A green lines). Note in the central schematic in Fig. 1A, that for the non-adapted condition the contrast drops down to 0 during the 4 s periods between 0.5 s tests, whereas during top-up conditions the contrast returns to 0.32 between tests. Furthermore, the initial 60 s of adaptation is not shown in this diagram. Low to medium contrasts were chosen for the adapting grating because our previous work indicated they produced reliable adaptation while still allowing the data to be easily fit with sigmoid curves (Stroud et al., 2012; LeDue et al., 2013).

Data analysis

Spikes were sorted offline with Spike2 software, which used a template-matching algorithm to identify spike waveforms, and then displayed candidate waveform clusters with a principle components analysis. Data from single units were then exported to MATLAB where neuronal responses were represented as spike density functions (SDFs) with 1 kHz resolution generated by

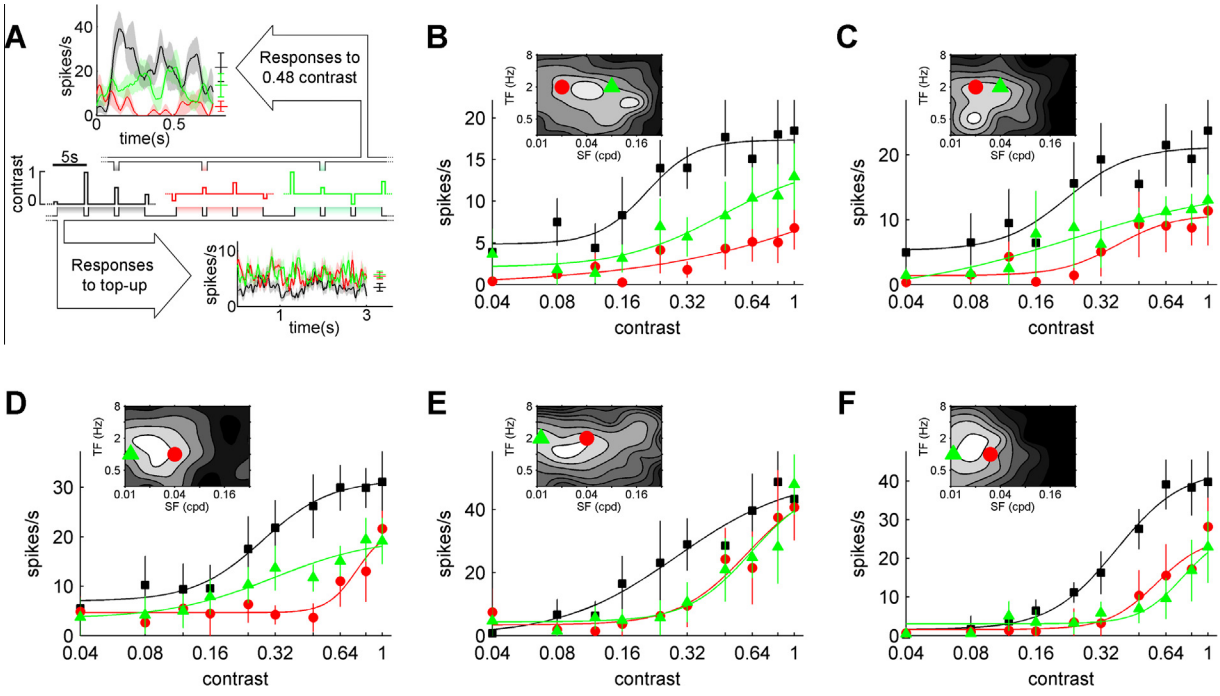

Fig. 1. Spatial Frequency specificity of top-up contrast adaptation. The central schematic in A shows short snippets of the non-adapted (black), matched adaptation (red), and nonmatched adaptation (green) stimuli containing several test contrasts interleaved with 0 contrast for the non-adapted condition or 0.32 contrast for adapted conditions. Spike density functions (SDFs) show a sample neuron's response to one test contrast (0.48; top left), and the last 3 s of the top-up period (bottom right) using the same color scheme. Average SDFs included all available repetitions, not just the snippets depicted in the schematic. Shaded regions of the SDFs indicate SEM. B–F show contrast response functions of five sample neurons with contrast on the abscissa and mean response rate on the ordinate. Non-adapted, matched adaptation, and nonmatched adaptation conditions are shown as black squares, red circles, and green triangles, respectively. Thin lines represent best fits to a sigmoid function (see Data analysis). Spatiotemporal tuning of each sample neuron is shown in the corresponding inset with spatial frequency (SF) in cycles per degree (cpd) on the abscissa and temporal frequency (TF) in hertz (Hz) on the ordinate. Contours with lighter shades of gray indicate higher firing rate. The SF and TF of the matched and nonmatched adapting stimuli are indicated with symbols corresponding to their respective contrast response functions. The neurons in D–F were selected because they had identical adapting SFs, yet they showed some diversity in their patterns of adaptation. All error bars represent 95% confidence intervals.

convolving a delta function at each spike arrival time with a Gaussian window.

Mean responses from top-up contrast response functions were fit to sigmoid curves using the least squares method (Albrecht and Hamilton, 1982):

$$R(c) = \frac{R_{max} \times c^n}{c^n + c_{50}^n} + M \quad (2)$$

where $R(c)$ is the amplitude of the evoked response at contrast c, M is baseline response to minimum contrast, n is the exponent that determines the steepness of the curve, R_{max} is the maximum elevation in response above the baseline, and c_{50} is the contrast that generates a response elevation of half R_{max}. Most non-adapted contrast response functions showed saturation allowing for well constrained fits, but saturation was less evident in the adapted responses. When fitting responses that did not saturate, we set upper and lower bounds on R_{max} of ±15% around the mean firing rate for contrasts between 0.82 and 1 in order to obtain tractable fits. Goodness of fit to the curves was measured using R^2 values, and the median R^2 value was 0.93. Proportional differences were calculated for c_{50} and R_{max} parameters ([adapted − non-adapted]/[adapted + non-adapted]) to normalize data between −1 and 1 for population analysis. Positive proportional differences in c_{50} indicate a rightward shift in the contrast response function, which is referred to as contrast gain control. Negative proportional differences in R_{max} indicate a downward shift in the contrast response function, which is referred to as response gain control (see Ibbotson, 2005 for a review).

We also calculated the area under the curve of each contrast response function to measure adaptation independent of sigmoid fits. This complementary analysis was unaffected by saturation, did not constrain the shape of the contrast response function, and though unable to distinguish contrast gain control from response gain control, it summarized adaptation-induced changes with a single term. Michelson contrast was first converted to percent contrast, then to log contrast, and then trapezoidal integration was performed on the log-contrast response function (Wissig and Kohn, 2012).

RESULTS

Contrast adaptation was measured in 67 visually responsive units in the primary visual cortex of 14 C57BL/6J mice. The preferred SFs ranged from 0.01 to 0.17 cpd (mean = 0.03 cpd) and preferred TFs ranged from 0.25 to 6.5 Hz (mean = 1.1 Hz), which were consistent with previous electrophysiological reports (Niell and Stryker, 2008; Gao et al., 2010; LeDue et al., 2012, 2013), and within the ranges indicated by recent multi-photon imaging studies (Andermann et al., 2011; Marshel et al., 2011). The proportion of neurons that gave phase-sensitive responses to a drifting grating of optimal SF was assessed by dividing the first Fourier coefficient of the response (F_1) by the mean time-averaged response (F_0; Skottun et al., 1991). However, measures of adaptation in our sample were not correlated with F_1/F_0 ratio, so all neurons were pooled for subsequent analysis.

Previous studies of mouse V1 have demonstrated substantial contrast adaptation following prolonged exposure to an adapting grating of the preferred SF and TF, and weaker adaptation elicited by adapting stimuli of non-preferred SFs or TFs (Stroud et al., 2012; LeDue et al., 2013). In this study, adapting SFs were selected not to generate maximum adaptation, but rather to produce similar spike rates between matched and non-matched adaptation. Care was taken to ensure adapting SFs were within the range of peak SFs reported in previous studies of V1, and below the mean SF cutoff measured for the dLGN and V1 (Grubb and Thompson, 2003; Gao et al., 2010; LeDue et al., 2012, 2013). Fig. 1 shows contrast adaptation data for six representative neurons. SDFs in Fig. 1A show two adapting SFs that elicited similar firing rates (lower right), but generated different amounts of adaptation (upper left). For the other example neurons (Fig. 1B-F), contrast response functions are shown for non-adapted (black squares), matched adaptation (red circles), and nonmatched adaptation (green triangles) conditions. The spatiotemporal tuning of each unit is summarized as a contour plot inset on the top left, and the SFs of the matched and nonmatched adapting gratings are indicated with corresponding symbols. The neurons in Fig. 1B–D showed greater changes when the SF of the adapting grating matched the SF of the test grating, and this pattern of results was most common in our data set. Fig. 1E shows a cell that adapted the same amount in both conditions, and Fig. 1F shows a neuron that adapted more after nonmatched adaptation.

Sigmoid fits to each contrast response function are shown as thin lines in Fig. 1, and the c_{50} and R_{max} parameters extracted from these fits were used to quantitatively analyze contrast gain control and response gain control following top-up adaptation. For the histograms in Fig. 2A–D, changes from the non-adapted curve were calculated as proportional differences in c_{50} and R_{max} between −1 and 1 (see Data analysis). Following matched adaptation, c_{50} values increased for 94% (63/67) of the sample (mean proportional difference = 0.20; Fig. 2A), whereas R_{max} values decreased for 88% (59/67) of the sample (mean proportional difference = −0.17; Fig. 2B). Following nonmatched adaptation, c_{50} values increased for a similar number of cells (93%; 62/67) but produced a slightly smaller mean proportional difference of 0.13 (Fig. 2C), whereas R_{max} values decreased for 93% of cells (62/67) and produced a similar mean proportional difference to matched adaptation (−0.21; Fig. 2D). We examined the proportional differences from non-adapted curves with t-tests (critical $p = 0.008$ with Bonferroni correction for multiple comparisons), and all were significantly different from zero (denoted by asterisks on Fig. 2A–D; all $p < 1.5 \times 10^{-8}$). It is clear that both matched and nonmatched adaptation generated substantial contrast gain control (positive proportional differences in c_{50}) and response gain control (negative proportional differences in R_{max}) relative to the non-adapted curves despite the fact they elicited sub-maximal firing rates.

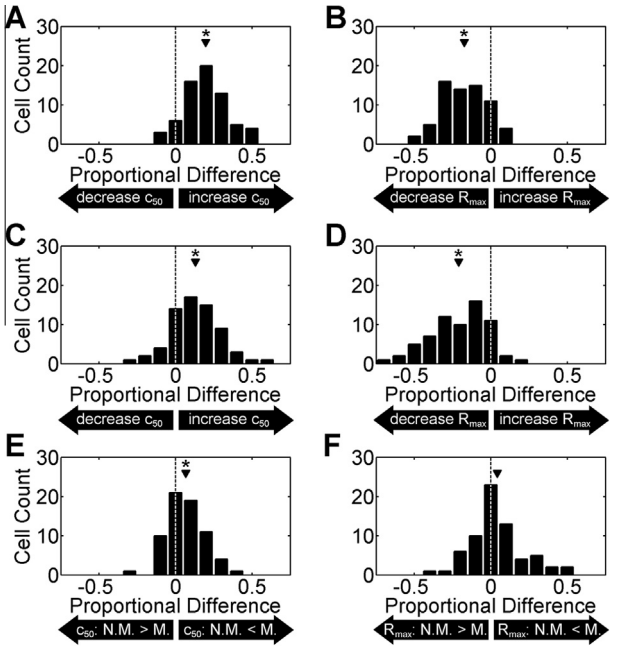

Fig. 2. Population data from top-up adaptation. Proportional differences were calculated for c_{50} (A, C, E) and R_{max} (B, D, F) parameters extracted from sigmoid fits. Matched (A) and nonmatched adaptation (C) caused c_{50} to increase for most neurons relative to non-adapted values, whereas matched (B) and nonmatched adaptation (D) caused R_{max} to decrease for most neurons relative to non-adapted values. The c_{50} (E) and R_{max} (F) values measured following matched (M) and nonmatched (N.M.) adaptation are also compared to each other directly. Solid triangles represent population means, and asterisks denote significant effects (see Results).

Fig. 2E, F compare matched and nonmatched adaptation directly by calculating the proportional difference between these two adapted conditions ([matched − nonmatched]/[matched + nonmatched]). Neurons had significantly higher c_{50}s following matched adaptation than nonmatched adaptation ($p = 6 \times 10^{-5}$; *t*-test), but this effect was modest with many values near zero and 67% (45/67) of neurons having positive proportional differences (mean = 0.07; Fig. 2E). A difference between R_{max} values from matched and nonmatched adaptation was not supported by our analysis ($p = 0.13$; *t*-test), and Fig. 2F shows that about half the proportional differences were positive (mean = 0.04).

A second analysis measuring changes in the area under the curves of each log-contrast response function was conducted to measure contrast adaptation independent of curve fitting (see Data analysis). Fig. 3A shows matched and nonmatched conditions normalized by the non-adapted area under the curve of each neuron (gray dots). The vast majority of normalized area values were smaller than 1, corroborating the robust adaptation measured for both matched and nonmatched conditions with curve fitting above. Furthermore, matched adaptation values (mean = 0.6) were significantly smaller than nonmatched (mean = 0.64; $p = 0.03$, paired *t*-test), and the 95% confidence limits for the difference between means did not overlap zero (0.006–0.08). Again, this small but significant difference suggests that matched adaptation usually induced more adaptation than nonmatched adaptation even when firing rates were approximately equal.

We calculated the proportional difference between the area under the curves of matched and nonmatched contrast response functions to get a single measure indicating which of the two conditions caused more adaptation in each neuron. This measure was not well correlated with the preferred SF ($r = 0.12$; $p = 0.32$), preferred TF ($r = -0.17$; $p = 0.15$), peak firing rate ($r = 0.02$; $p = 0.87$), orientation tuning ([(preferred − orthogonal)/(preferred + orthogonal)]; $r = 0.062$; $p = 0.71$), or whether the test SF was the higher or lower of the two adapting SFs ([log(matched SF/nonmatched SF)]; $r = 0.02$; $p = 0.86$). However, to further explore the relationship between firing rate and adaptation we pooled our current data set with one from LeDue et al. (2013), and compared the proportional differ-

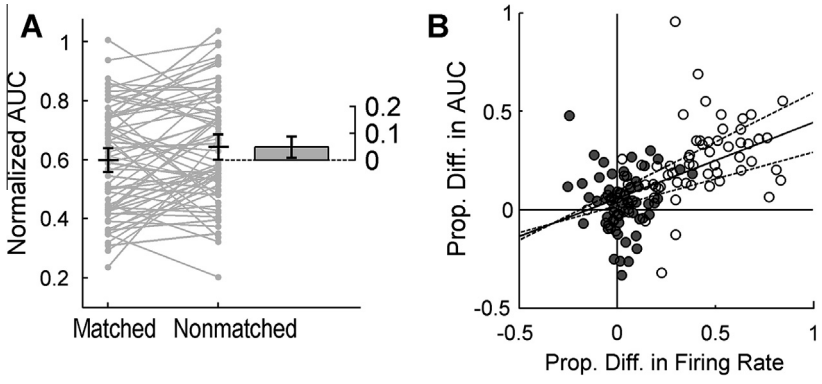

Fig. 3. Area under the curve analysis of contrast adaptation. The gray dot-pairs in A show matched and nonmatched conditions normalized by the non-adapted area under the curve (AUC) of each neuron. The sample mean and 95% confidence intervals for each condition are shown in black. The difference between conditions is shown to the right, with error bars indicating the 95% confidence intervals for the difference between means. The scatter graph in B plots the proportional difference in firing rate elicited by the adapting gratings (abscissa) against the proportional difference between the area under the curves of matched and nonmatched contrast response functions (ordinate). Gray dots show data from the current study and empty dots show the data from LeDue et al. (2013). The solid diagonal line shows the line of best fit from a linear regression, and dashed lines indicate the 95% confidence limits of the fit.

ence in firing rate elicited by the adapting gratings with the proportional difference between the area under the curves of matched and nonmatched contrast response functions. Gray dots in Fig. 3B show data from the current study where we attempted to match the firing rates elicited by both adapting gratings. Empty dots show the data from LeDue et al. (2013) where the matched grating was of the preferred SF, and the nonmatched grating had an SF that was 2–3 octaves higher or lower (and hence the conditions induced substantially different firing rates). Here, a hypothetical neuron that responded much more strongly to the matched adaptor and also showed greater adaptation to this condition would have large positive values for both the abscissa and ordinate. A liner regression of the total data set revealed a strong relationship between the differences in firing rate elicited by the two adaptors and the amount of adaptation produced by each ($r = 0.52$, $p < 0.0001$). The y-intercept of the regression line was 0.06 (95% confidence limits between 0.02 and 0.1) indicating that matched adaptation should induce slightly more adaptation than nonmatched adaptation when there is no difference in firing rate, and this is exactly what our other analyses indicated as well.

DISCUSSION

During visual adaptation the neural processing of a stimulus is shaped by recent stimulus history, which provides the opportunity to link alterations in perception with underlying transient neural changes. Perceptual studies of contrast adaptation indicate that it is pattern-specific (first described by Blakemore and Campbell, 1969a,b), but the neural basis for this specificity is not well understood. In this study we demonstrated that contrast adaptation in many mouse V1 neurons showed some degree of SF specificity even when both adapting stimuli evoked approximately the same firing rate. These observations augment and extend previous work that examined pattern specificity of contrast adaptation in mouse V1 (LeDue et al., 2013).

Comparisons with previous studies

Using a virtually identical stimulus and analysis to the current study, LeDue et al. (2013) tested mouse V1 neurons at their preferred SF and found that contrast adaptation was stronger when the adapting SF matched the test SF than when the adapting and test SFs differed by 2–3 octaves. By virtue of the sharp spatiotemporal tuning of most V1 neurons (Andermann et al., 2011; LeDue et al., 2012; Fig. 1 insets), the peak SF also usually elicited substantially higher spike rates than the off-peak SF. The pooled analysis of the current data set and LeDue et al. (2013) demonstrated that when the matched condition induced higher firing rates there was greater matched adaptation compared to nonmatched adaptation (Fig. 3B), which indicates that an intrinsic or fatigue-like process probably contributes a great deal to the SF specificity of adaptation in most circumstances. In fact, the linear relationship between relative firing rate induced by two adapting stimuli and the resultant adaptation produced makes it straightforward to predict stimuli that will induce relatively more adaptation in a neuron if its SF tuning is known. However, when spike rates elicited by the two adapting stimuli were about equal, matched adaptation was still stronger than nonmatched adaptation (i.e. the positive *y*-intercept in Fig. 3B), indicating there is a small remaining component of SF specificity that must arise extrinsically to the recorded neuron. This modest amount of specificity could be amplified at subsequent stages, similar to how the subtle orientation bias of dLGN afferents can be amplified to robust orientation tuning in V1 (Scholl et al., 2013).

The first electrophysiological studies of the SF specificity of contrast adaptation in cats did not overtly attempt to distinguish intrinsic from extrinsic sources of adaptation. Movshon and Lennie (1979) demonstrated that matched adaptation was stronger than nonmatched adaptation using a top-up protocol similar to the one in our current work. The firing rates elicited by each SF were somewhat similar in the single example neuron shown, hinting that SF specificity in cat V1 may also have an extrinsic source (their Fig. 3), but the lack of population data for firing rate makes this hard to confirm. Albrecht et al. (1984) used a preferred adapting SF and several different test SFs for each neuron to convincingly demonstrate that contrast adaptation is SF specific, but this design difference allows for only indirect comparisons with our data. One study of cat dLGN that did explicitly attempt to equate the firing rates elicited by matched and nonmatched adapting SFs found no SF specificity of contrast adaptation (Duong and Freeman, 2007). This, along with previous evidence that adaptation in dLGN is weaker than in V1 (Ohzawa et al., 1985; Sanchez-Vives et al., 2000a), confirms that V1 is the most logical place to look for mechanisms contributing to SF specificity of contrast adaptation.

Potential mechanisms of adaptation

Intracellular electrophysiological studies in cats have implicated a Na^+-dependent K^+ current that produces hyperpolarization of the membrane potential as one biophysical substrate of the fatigue-like effects observed following contrast adaptation. However, since visual adaptation decreased neuronal firing much more than a current injection that mimicked this hyperpolarization, it was acknowledged that other sources of adaptation must also be accounted for (Sanchez-Vives et al., 2000a,b; Carandini, 2000). Our results in mouse are consistent with an intrinsic source of adaptation playing a large role in SF specificity, but additional experiments are required to test whether it is implemented by similar mechanisms.

Divisive normalization implemented by a local pool of neurons has been proposed as an extrinsic source of adaptation (Heeger, 1992; Dhruv et al., 2011). If this normalization pool indiscriminately integrates signals from a local network of neurons (Dragoi et al., 2001; Levy et al., 2014), it could partially explain differences in the orientation and SF specificity of contrast adaptation observed in mouse V1. In cat V1, neurons with similar preferences cluster together forming orientation columns

(Hubel and Wiesel, 1974; Ohki et al., 2006), and it has been suggested that contrast adaptation is orientation specific in iso-orientation domains where the local network prefers a single orientation, but not in pinwheel centers where the local network contains varied orientation preferences (Crowder et al., 2006, but see Sengpiel and Bonhoeffer, 2002). Mice lack orientation columns (Ohki et al., 2006), and contrast adaptation is not orientation specific in this species (Stroud et al., 2012). Contrary to orientation, columnar organization of SF preference has been reported in both cats (Shoham et al., 1997; Ribot et al., 2013) and mice (Ji et al., 2015), and the inclusion of clustered SF preferences in the normalization pool could contribute to the SF specificity of contrast adaptation found in both cat and mouse V1.

Other potential extrinsic sources of adaptation include inheritance from pre-cortical stages (retina: reviewed in Demb, 2008; dLGN: Sanchez-Vives et al., 2000a; Solomon et al., 2004; Duong and Freeman, 2007), and synaptic depression at the thalamo-cortical synapse (Chung et al., 2002). Thus, there remain many open questions about the mechanisms that contribute to adaptation, their relative contributions, and the stage at which each one is implemented. The genetic tools available in mice provide additional avenues of investigation for these questions. Despite differences in eye position, circadian cycle, and spatial acuity among animal models, contrast adaptation in mouse visual cortex appears to share many similarities with adaptation described in cats and primates. Therefore, we are optimistic that working to understand adaptation in the mouse model will provide relevant insights into processes occurring in higher mammals.

AUTHOR CONTRIBUTIONS

J.L.K., M.P.L. and N.A.C. all collected data, analyzed data, and wrote and edited the manuscript.

Acknowledgements—This work was supported by the Natural Sciences and Engineering Research Council of Canada (NSERC) and the Canada Foundation for Innovation (CFI). NSERC and CFI had no influence on the study design, analysis, or writing of the report.

REFERENCES

Abbonizio G, Langley K, Clifford CWG (2002) Contrast adaptation may enhance contrast discrimination. Spat Vis 16:45–58.
Albrecht DG, Hamilton DB (1982) Striate cortex of monkey and cat: contrast response function. J Neurophysiol 48:217–237.
Albrecht DG, Farrar SB, Hamilton DB (1984) Spatial contrast adaptation characteristics of neurones recorded in the cat's visual cortex. J Neurophysiol 347:713–739.
Andermann ML, Kerlin AM, Roumis DK, Glickfeld LL, Reid RC (2011) Functional specialization of mouse higher visual cortical areas. Neuron 72:1025–1039.
Blakemore C, Campbell F (1969a) Adaptation to spatial stimuli. J Physiol 200:11–13.
Blakemore C, Campbell F (1969b) On the existence of neurones in the human visual system selectively sensitive to the orientation and size of retinal images. J Physiol 203:237–260.
Blakemore C, Nachmias J (1971) The orientation specificity of two visual after-effects. J Physiol 213:157–174.
Blakemore C, Muncey JP, Ridley RM (1973) Stimulus specificity in the human visual system. Vision Res 13:1915–1931.
Bonds A (1991) Temporal dynamics of contrast gain in single cells of the cat striate cortex. Vis Neurosci 6:239–255.
Brainard DH (1997) The psychophysics toolbox. Spat Vis 10:433–436.
Carandini M (2000) Visual cortex: fatigue and adaptation. Curr Biol 10:R605–R607.
Chung S, Li X, Nelson SB (2002) Short-term depression at thalamocortical synapses contributes to rapid adaptation of cortical sensory responses in vivo. Neuron 34:437–446.
Crowder NA, Price NSC, Hietanen M, Dreher B, Clifford CWG, Ibbotson MR (2006) Relationship between contrast adaptation and orientation tuning in V1 and V2 of cat visual cortex. J Neurophysiol 95:271–283.
Demb JB (2008) Functional circuitry of visual adaptation in the retina. J Physiol 586:4377–4384.
Dhruv NT, Tailby C, Sokol SH, Lennie P (2011) Multiple adaptable mechanisms early in the primate visual pathway. J Neurosci 31:15016–15025.
Dragoi V, Rivadulla C, Sur M (2001) Foci of orientation plasticity in visual cortex. Nature 411:80–86.
Duong T, Freeman RD (2007) Spatial frequency-specific contrast adaptation originates in the primary visual cortex. J Neurophysiol 98:187–195.
Foley JM, Chen CC (1997) Analysis of the effect of pattern adaptation on pattern pedestal effects: a two-process model. Vision Res 37:2779–2788.
Gao E, DeAngelis GC, Burkhalter A (2010) Parallel input channels to mouse primary visual cortex. J Neurosci 30:5912–5926.
Greenlee M, Heitger F (1988) The functional role of contrast adaptation. Vision Res 28:791–797.
Grubb MS, Thompson ID (2003) Quantitative characterization of visual response properties in the mouse dorsal lateral geniculate nucleus. J Neurophysiol 90:3594–3607.
Heeger DJ (1992) Normalization of cell responses in cat striate cortex. Vis Neurosci 9:181–197.
Hubel DH, Wiesel TN (1974) Sequence regularity and geometry of orientation columns in the monkey striate cortex. J Comp Neurol 158:267–293.
Ibbotson MR (2005) Physiological mechanisms of adaptation in the visual system. In: Clifford CWG, Rhodes G, editors. Fitting the mind to the world: adaptation and aftereffects in high-level vision. Oxford: Oxford University Press. p. 17–45.
Ji W, Gămănuţ R, Bista P, D'Souza RD, Wang Q, Burkhalter A (2015) Modularity in the organization of mouse primary visual cortex. Neuron 87:632–643.
Kalatsky VA, Stryker MP (2003) New paradigm for optical imaging: temporally encoded maps of intrinsic signal. Neuron 38:529–545.
Kaplan E, Shapley RM (1986) The primate retina contains two types of ganglion cells, with high and low contrast sensitivity. Proc Natl Acad Sci USA 83:2755–2757.
Kohn A (2007) Visual adaptation: physiology, mechanisms, and functional benefits. J Neurophysiol 97:3155–3164.
LeDue EE, Zou MY, Crowder NA (2012) Spatiotemporal tuning in mouse primary visual cortex. Neurosci Lett 528: 165–169.
LeDue EE, King JL, Stover KR, Crowder NA (2013) Spatiotemporal specificity of contrast adaptation in mouse primary visual cortex. Front Neural Circuits 7:154.
Levy M, Lu Z, Dion G, Kara P (2014) The shape of dendritic arbors in different functional domains of the cortical orientation map. J Neurosci 34:3231–3236.
Marshel JH, Garrett ME, Nauhaus I, Callaway EM (2011) Functional specialization of seven mouse visual cortical areas. Neuron 72:1040–1054.
Movshon JA, Lennie P (1979) Pattern-selective adaptation in visual cortical neurones. Nature 278:850–852.
Niell CM, Stryker MP (2008) Highly selective receptive fields in mouse visual cortex. J Neurosci 28:7520–7536.

Ohki K, Chung S, Kara P, Hübener M, Bonhoeffer T, Reid RC (2006) Highly ordered arrangement of single neurons in orientation pinwheels. Nature 442:925–928.
Ohzawa I, Sclar G, Freeman RD (1982) Contrast gain control in the cat visual cortex. Nature 298:266–268.
Ohzawa I, Sclar G, Freeman RD (1985) Contrast gain control in the cat's visual system. J Neurophysiol 54:651–667.
Paxinos G, Franklin K (2001) The mouse brain in stereotaxic coordinates. 2nd ed. San Diego: Academic Press.
Pelli D (1997) The video tookbox software for visual psychophysics: transforming numbers into movies. Spat Vis 10:437–447.
Ribot J, Aushana Y, Bui-Quoc E, Milleret C (2013) Organization and origin of spatial frequency maps in cat visual cortex. J Neurosci 33:13326–13343.
Sanchez-Vives M, Nowak L, McCormick D (2000a) Membrane mechanisms underlying contrast adaptation in cat area 17 in vivo. J Neurosci 20:4267–4285.
Sanchez-Vives M, Nowak L, McCormick D (2000b) Cellular mechanisms of long-lasting adaptation in visual cortical neurons in vitro. J Neurosci 20:4286–4299.
Saul A, Cynader M (1989) Adaptation in single units in visual cortex: the tuning of aftereffects in the spatial domain. Vis Neurosci 2:593–607.
Scholl B, Tan AY, Corey J, Priebe NJ (2013) Emergence of orientation selectivity in the Mammalian visual pathway. J Neurosci 33:10616–10624.
Sclar G, Lennie P, DePriest DD (1989) Contrast adaptation in striate cortex of macaque. Vision Res 29:747–755.
Sengpiel F, Bonhoeffer T (2002) Orientation specificity of contrast adaptation in visual cortical pinwheel centres and iso-orientation domains. Eur J Neurosci 15:876–886.
Shoham D, Hübener M, Schulze S, Grinvald A, Bonhoeffer T (1997) Spatio-temporal frequency domains and their relation to cytochrome oxidase staining in cat visual cortex. Nature 385:529–533.
Skottun BC, De Valois RL, Grosof DH, Movshon JA, Albrecht DG, Bonds AB (1991) Classifying simple and complex cells on the basis of response modulation. Vision Res 31:1079–1086.
Snowden RJ, Hammett ST (1996) Spatial frequency adaptation: threshold elevation and perceived contrast. Vision Res 36:1797–1809.
Solomon SG, Peirce JW, Dhruv NT, Lennie P (2004) Profound contrast adaptation early in the visual pathway. Neuron 42:155–162.
Stroud AC, Ledue EE, Crowder NA (2012) Orientation specificity of contrast adaptation in mouse primary visual cortex. J Neurophysiol 108:1381–1391.
Vautin RG, Berkley MA (1977) Responses of single cells in cat visual cortex to prolonged stimulus movement: neural correlates of visual aftereffects. J Neurophysiol 40:1051–1065.
Wang Q, Burkhalter A (2007) Area map of mouse visual cortex. J Comp Neurol 357:339–357.
Wissig SC, Kohn A (2012) The influence of surround suppression on adaptation effects in primary visual cortex. J Neurophysiol 107:3370–3384.

(Accepted 11 September 2015)
(Available online 18 September 2015)